

## Long-term analysis of clear nights using satellite data considering astronomical sites in western China

Zi-Huang Cao<sup>1,2</sup>, Li-Yong Liu<sup>1</sup>, Yong-Heng Zhao<sup>1,2</sup>, Lu Feng<sup>1</sup>, Hugh R. A. Jones<sup>4</sup>, Huang Shen<sup>5</sup>, Jin-Xin Hao<sup>1</sup>, Yan-Jie Xue<sup>1</sup>, Yong-Qiang Yao<sup>1</sup>, Jing Xu<sup>2,6</sup>, Ali Esamdin<sup>2,6</sup>, Zhao-Xiang Qi<sup>2,3</sup>, Jian-Rong Shi<sup>1,2</sup>, Jian Li<sup>1</sup>, Yuan Tian<sup>1</sup>, Zheng Wang<sup>1,2</sup>, Tai-Sheng Yan<sup>2</sup>, Xia Wang<sup>1</sup>, Jian-Ping Xiong<sup>2</sup>, Si-Cheng Yu<sup>1</sup>, Jun-Bo Zhang<sup>1</sup>, Zhi-Xia Shen<sup>1</sup>, Yun-Ying Jiang<sup>1</sup>, Jia Yin<sup>1</sup>, Guang-Xin Pu<sup>6</sup>, Peng Wei<sup>6</sup>, Chun-Hai Bai<sup>6</sup>, Guo-Jie Feng<sup>2,6</sup>, Lu Ma<sup>6</sup>, Teng-Fei Song<sup>7</sup>, Jian-Feng Wang<sup>1</sup>, Jian-Feng Tian<sup>1</sup>, Xian-Qun Zeng<sup>1</sup>, Zhi-Gang Hou<sup>1</sup>, Shi-Long Liao<sup>2</sup>, Zhi-Song Cao<sup>1</sup>, Dong-Wei Fan<sup>1</sup>, Yun-Fei Xu<sup>1,2</sup>, Chang-Hua Li<sup>1</sup> and Yi-Han Tao<sup>1</sup>

<sup>1</sup> National Astronomical Observatories, Chinese Academy of Sciences, Beijing 100101, China; [zhcao@bao.ac.cn](mailto:zhcao@bao.ac.cn)

<sup>2</sup> University of Chinese Academy of Sciences, Beijing 100049, China

<sup>3</sup> Shanghai Astronomical Observatory, Chinese Academy of Sciences, Shanghai 200030, China

<sup>4</sup> Centre for Astrophysics, University of Hertfordshire, Hatfield, UK

<sup>5</sup> School of Journalism, Communication University of China, Beijing 100024, China

<sup>6</sup> Xinjiang Astronomical Observatory, Chinese Academy of Sciences, Urumqi 830011, China

<sup>7</sup> Yunnan Observatories, Chinese Academy of Sciences, Kunming 650216, China

Received 2019 September 2; accepted 2020 January 30

**Abstract** A large ground-based optical/infrared telescope is being planned for a world-class astronomical site in China. The cloud-free night percentage is the primary meteorological consideration for evaluating candidate sites. The data from GMS and NOAA satellites and the MODIS instrument were utilized in this research, covering the period from 1996 to 2015. Our data analysis benefits from overlapping results from different independent teams as well as a uniform analysis of selected sites using GMS+NOAA data. Although significant ground-based monitoring is needed to validate these findings, we identify three different geographical regions with a high percentage of cloud-free conditions ( $\sim 83\%$  on average), which is slightly lower than at Mauna Kea and Cerro Armazones ( $\sim 85\%$  on average) and were chosen for the large international projects TMT and ELT respectively. Our study finds evidence that cloud distributions and the seasonal changes affected by the prevailing westerly winds and summer monsoons reduce the cloud cover in areas influenced by the westerlies. This is consistent with the expectations from climate change models and is suggestive that most of the identified sites will have reduced cloud cover in the future.

**Key words:** methods: statistical — site testing — atmospheric effects — MODIS

### 1 INTRODUCTION

The Large Optical/Infrared Telescope (Cui et al. 2018) is a proposed ground-based general-purpose telescope with a 12 m aperture and adaptive-optics system. The project has not only a developed engineering design for the telescope but also the associated scientific goals, related to the instruments and observation modes. Referring to the experience gained from studies of the Thirty Meter Telescope (TMT) (Schöck et al. 2011) and the Extremely Large Telescope (ELT) (Melnick & Monnet 2011), the percentage of clear

nights is the most straightforward and high-priority parameter in the site merit function (Schöck et al. 2009). However, the definition of “clear” is indistinct. Different instruments have different interpretations regarding clouds, and furthermore the fractions of photometric time and of “usable” time (spectroscopic) need to be well defined and calibrated with respect to ground-based data in a manner similar to that laid out by Cavazzani et al. (2011).

The definition of “clear” is based on different kinds of measurements at different wavelengths and so has a differ-

ent meaning in different datasets. In this study, although the definition of “clear” is critical for processing and analysis, self-consistency and long-term comparability are also important for all datasets. One method to increase the clarity of results would be to consider clear sky percentages in daytime as well as nighttime. For satellites, sunlight increases the temperature of the surface, which could affect the results of cloud cover. For ground-based observation, sunlight significantly increases the contrast of cloud edges and moonlight at night could enhance or weaken the potential for cloud identification depending on apparatus, e.g., naked-eye or all-sky camera. Cavazzani et al. (2015) indicate that the difference between day and night is not significant based on 2003 to 2012 data from Moderate Resolution Imaging Spectroradiometer (MODIS) targeting at Paranal, La Silla and Mt Graham. However, it is important to realize that Cavazzani et al.’s analysis highlighted the need to adjust the pixel position for Paranal in order not to mix the contribution of ocean and land in the same pixel. On the other hand, at a location with very different geography, Barnes et al. (2016) reported a non-negligible difference from the analysis of Hawaiian Island cloud cover from 2001 to 2011 based on the same satellites. For more reliable results on our less studied sites, we only process and compare nighttime data.

Our analysis considers a range of different potential sites largely selected based on historical experiments and includes existing observatories. Most of the sites are located west of  $100^\circ$  E and north of  $40^\circ$  N. The site altitudes are mostly higher than 4500 m, and all sites are on mountains or highlands hundreds of meters above the average local altitude. All would appear to be feasible sites for constructing a large telescope. Except for the sites in group C, all locations have All-Sky Cameras and Differential Image Motion Monitors operated by Chinese Academy of Sciences.

In order to facilitate comparison between regions, the reference sites are divided into groups based on geographic locations. Nearby sites are grouped together, and existing observatories are all assigned to the last group (E). The order of the groups from A to D is according to longitude from west to east, and the site order in the group is according to latitude from south to north. Information about the sites and groups is listed in Table 1.

Research on night cloud cover from the meteorological stations’ climate data was finished by Qian et al. (2012). Two large areas with low cloud cover are located in China as illustrated in Figure 1, distinguished by the 35% contour line. These cloud-free areas are roughly consistent with previous analyses, e.g., Huang & Mao (1994) and

**Table 1** Position, Altitude and Group are listed for all sites referred to in this work.

Site	Longitude (degree)	Latitude (degree)	Altitude (meter)	Group
Muztagh-ata	74.89676	38.33044	4526	A
Xiangzi	79.85360	31.86121	4836	B
Diya	78.99159	31.89757	5143	B
Ali-F	80.33494	32.15154	5125	B
Ali-D	80.13346	32.25783	5292	B
Ali-A	80.02671	32.32573	5040	B
Payang	83.46912	30.04289	4600	C
Huoerba	83.03725	30.20617	4621	C
Daocheng	100.10890	29.10695	4739	D
Delingha	97.72969	37.37794	3208	E
Gaomeigu	100.02935	26.69378	3216	E
Nanshan	87.17952	43.47178	2067	E
Xinglong	117.57744	40.39555	882	E

Zhang et al. (2010). East of the 35% contour line, including part of Inner Mongolia, Hebei province and Northeast China, the wind speed is relatively high, there is more dusty weather and severe light pollution is associated with intensive human activities. Furthermore, this situation is getting worse with the rapid development of the Chinese economy. In western China, especially inside the 35% contour line, there is a relatively high percentage of areas with clear nights and low population density, including highlands, the Gobi Desert and mountains. All these areas are suitable for a variety of astronomical observations.

As early as the 1980s, surveys of astronomical sites concentrated on western China, and four new observatories resulted from those surveys, including Delingha in Qinghai from 1983 (Tian et al. 2016), Nanshan in Xinjiang from 1991 (Liu et al. 2013) and Gaomeigu in west Yunnan from 1995 (Chen et al. 2003). The geographical distribution of these sites is from  $87^\circ$  E to  $101^\circ$  E, and the altitudes of these sites are from 2067 to 3216 m above sea level, systematically further west and higher than previously existing observatories in China like Xinglong (Zhang et al. 2015). Thus, these observatories serve as a comparative sample for further site testing. The contours of all our sites are plotted in Figure 1. The remainder of this paper is arranged as follows. The description, processing and results of the satellite data are covered in Section 2, and Section 3 concludes our work.

## 2 CLOUD COVER BASED ON SATELLITE DATA

Meteorological satellites use specific cloud-sensitive spectral ranges (e.g., Ackerman et al. 1998; Frey et al. 2008) to measure radiation emitted or reflected by the Earth’s surface or atmospheric systems on Earth (e.g., Menzel et al. 2008), and then to convert the measured radiation to cloud parameters. The inversion of cloud parameters gen-

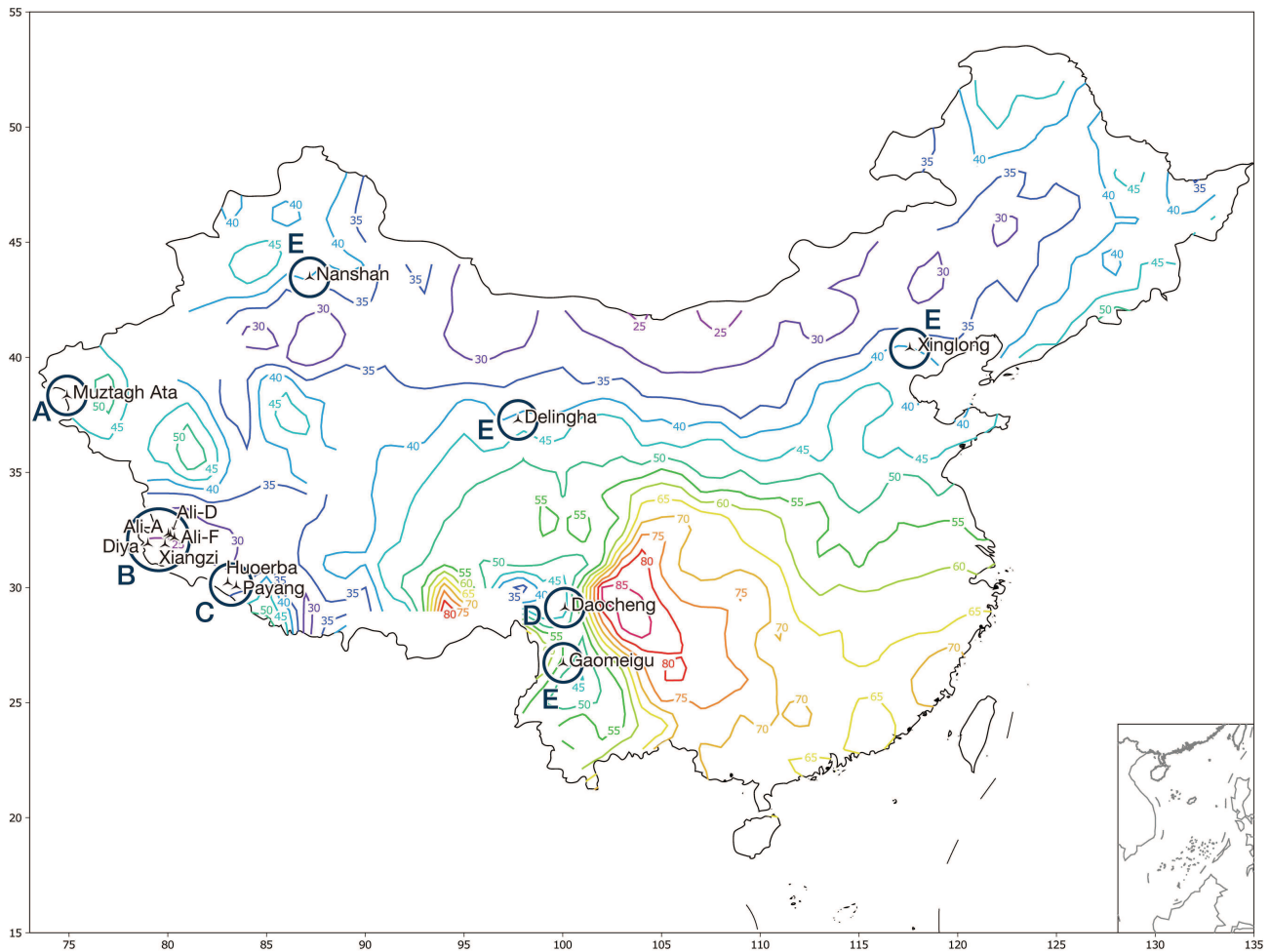


**Fig. 1** The distribution of cloud cover recorded at meteorological stations accumulated from 1961 to 2008. The data are from the National Meteorological Information Center of China Meteorological Administration and include climate data from 727 meteorological stations. The cloud cover is observed by naked eye, with a standard from 0 to 10, corresponding to a clear sky and all-sky clouds with a stated accuracy of 10%, and directly converting the 0–10 naked-eye scale into a percentage. The cloud observations are performed four times a day, and the data at 2:00 AM Beijing time are employed for our nighttime cloud cover analysis. The abscissa represents longitude, and the ordinate signifies latitude. The unit of a geographic location is degree. The marks on the contour lines represent the annual percentage of the night cloud cover. The locations of sites and groups are plotted in the figure and listed in Table 1 (Qian et al. 2012).

erally involves two steps: (1) cloud detection where cells are divided into cloud and clear sky cells, (2) parameter estimation where a variety of mathematical methodologies are employed to infer cloud parameters (e.g., Barnes et al. 2016; Liu & Liu 2013).

While ground-based data will be vital for final site choices, meteorological satellite data can significantly reduce the requirement for site testing with ground-based observations and provide a broad range of uniform measurements yielding multi-era cloud data. The long-time span of satellite data provides the possibility for in-depth analysis and study of cloud cover. Parts of datasets from the International Satellite Cloud Characterization Program (ISCCP), GMS+MODIS, GMS+NOAA and MODIS-ST

from 1996 to 2015 (e.g., Stubenrauch et al. 2013) are utilized in this study.

## 2.1 Cloud Cover Based on GMS+NOAA Data

### 2.1.1 GMS+NOAA data description

The GMS satellite is a geosynchronous satellite, positioned at  $140^{\circ}$  E over the equator. The Stretched Visible and Infrared Spin Scan Radiometer (SVISSR) on GMS consists of four channels, including visible ( $0.55\text{--}0.90\ \mu\text{m}$ ), near-infrared ( $1.628\text{--}1.625\ \mu\text{m}$ ) and infrared ( $10.5\text{--}11.5\ \mu\text{m}$  and  $11.5\text{--}12.5\ \mu\text{m}$ ) (Kramer 2002). The pixel resolution for GMS/SVISSR at infrared channels is 5 km at nadir (Dim et al. 2007) and drops to 20 km at the edge (Huang & Mao 1996).

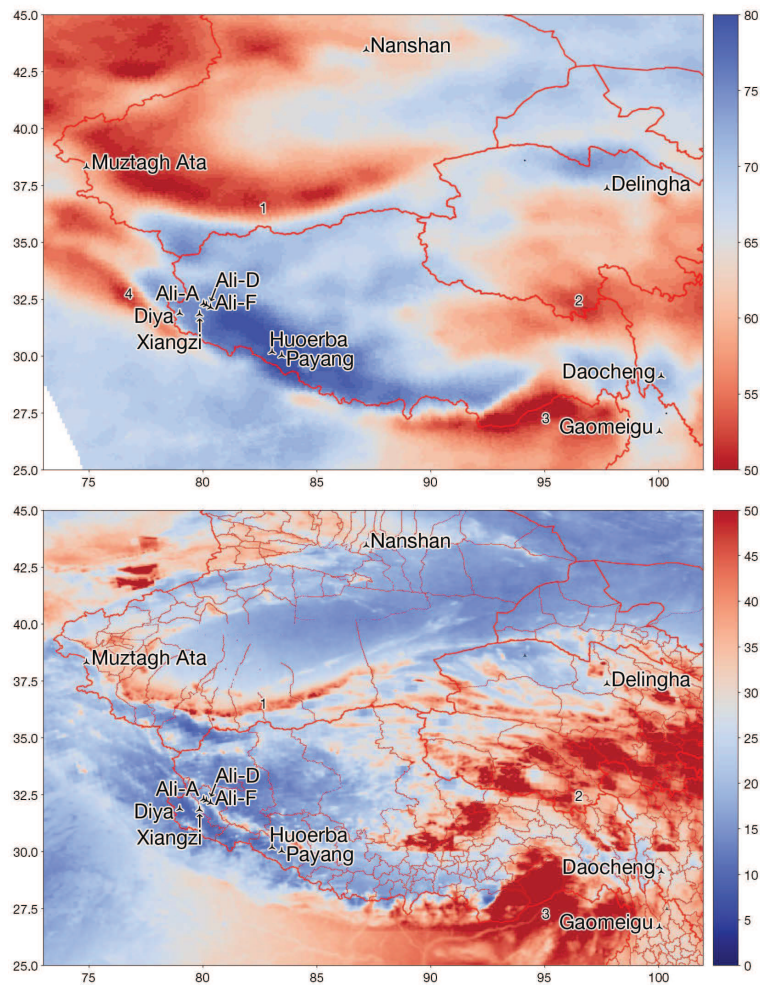


**Fig. 2** The percentage distribution of GMS+NOAA clear nights accumulated from 1996 to 2003 for western China is in the *upper panel* of the figure. The abscissa represents longitude, and the ordinate signifies latitude. The color scale is from 50 to 80, chosen to easily distinguish the most promising regions. In both panels, the *thick red lines* trace the country borders, the *thinner red lines* mark provincial and city borders and the *thin red lines* are rivers. The percentage distribution of cloudy nights less than 50% accumulated from 2003 January 1 to 2015 December 31 for national and western China from MODIS data is in the *lower panel* of the figure. The abscissa represents longitude, and the ordinate corresponds to latitude. The borders are roughly aligned with GMS+NOAA data, moreover, the color scale is from 0 to 50 and is chosen so as to optimize visual comparison with the GMS+NOAA data.

NOAA satellites are polar-orbiting meteorological satellites. The 1st and 2nd generations of Advanced Visible and High-Resolution Radiometer (NOAA/AVHRR1 and NOAA/AVHRR2) on these NOAA satellites consist of five channels, including (0.55–0.68  $\mu\text{m}$ ), near-infrared (0.725–1.10  $\mu\text{m}$  and 3.55–3.93  $\mu\text{m}$ ), and infrared (10.3–11.3  $\mu\text{m}$  and 11.5–12.5  $\mu\text{m}$ ), and the pixel resolutions at nadir for NOAA/AVHRR1 and NOAA/AVHRR2 are 1.1 km (Chen 2017).

The data presented in this paper were processed following the scheme devised by Huang & Mao (1996). The 90% pixels were processed by the time standard and spatial standard from the ISCCP (Rodgers 1976) and the rest were processed by an appendix threshold standard defined by Huang & Mao (1996). In total, 43 766 images from

1996 to 2004 were processed and provide 12 km resolution. Considering the GMS spatial resolution in western China is about 20 km, (Mao, private communication), these data were conservatively binned in the dataset by a factor of three to yield uniform  $36 \times 36 \text{ km}^2$  elements, each supplied with a clear night percentage based on the number of clear hours divided by the total hours between astronomical twilight.

### 2.1.2 GMS+NOAA data results

From GMS+NOAA data, there are four areas with high cloud cover marked in Figure 2 and described in Table 2, centered on the Tibetan Plateau in western China.

**Table 2** Areas in Western China with a Low Clear Night Fraction Based on GMS+NOAA

Mark	Region	Cause
1	The northwestern side of the Tibetan Plateau and the southern margin of the Tarim Basin.	From the Pamir wet area, the westerlies over the Pamir Plateau form clouds, with anticyclone circulation from the Tarim Basin (Dai 1990; Weng & Han 1998).
2	The eastern side of the Tibet Plateau, Sichuan, Yunnan and Guizhou.	A southwest low vortex system forms clouds, and the intersection of the southwest jet and the northwest jet produces weather systems (Liu et al. 2003).
3	The Great Bend of Yarlung Zangbo.	From the Pamir wet area, combined with water vapor from Yarlung Zangbo and the Indian Ocean, westerlies climb up and form clouds on the windward side (Liu et al. 2003).
4	The west side of the Tibetan Plateau.	From the Pamir wet area, westerlies climb up and form clouds on the windward side (Liu et al. 2003).

On a large scale, China has two main areas which are consistent with the historical ground-based observations and offer a high number of clear nights: (1) The vicinity of  $40^\circ$  N, extending from central Inner Mongolia to central Xinjiang. (2) The western and southwestern parts of the Tibetan Plateau from  $78^\circ$  E to  $95^\circ$  E. Two areas with low cloud cover are located near  $100^\circ$  E. One is between Yunnan and Sichuan, with latitudes between  $25^\circ$  N and  $30^\circ$  N, and the other is northern Qinghai, with latitudes ranging from  $35^\circ$  N to  $40^\circ$  N. Due to topography, the potential area for astronomical sites in western Xinjiang to the Kazakhstan border is significantly reduced. However, we should note that GMS+NOAA data are not recent and have relatively low spatial resolution, which in a mountainous area may decrease the accuracy of the specific site's cloud cover measurements. We note that the closest snow-covered mountain is 11 km from the Muztagh-ata site and so  $36 \times 36 \text{ km}^2$  resolution does not satisfy the cloud cover research for each site. Although the work of Cavazzani et al. (2015) suggests that snow cover is likely to significantly perturb the measurements, it may not be indicative of a bad locale per se since, for example, the literal translation of Mauna Kea is white mountain in reference to its occasional snow covering. Therefore, higher resolution satellite data are needed.

## 2.2 Cloud Cover Based on MODIS Data

### 2.2.1 MODIS data description

The Earth Observing System (EOS) project was started by the National Aeronautics and Space Administration (NASA) in the United States in 1999, and included EOS/TERRA and EOS/AQUA satellites. MODIS<sup>1</sup> on EOS/TERRA and EOS/AQUA has 36 spectral channels in  $0.4\text{--}14 \mu\text{m}$  across the visible and infrared regions. The resolutions at nadir depend on the channels, includ-

ing 0.25 km for channels 1–2, 0.5 km for channels 3–7 and 1 km for channels 8–36 (Chen 2017). The polar-orbiting satellites EOS/TERRA and EOS/AQUA observe the Earth four times a day at local times around 10:30 AM, 1:30 PM, 10:30 PM and 1:30 AM (Platnick et al. 2003).

The National Meteorological Center of China processed the MODIS satellite data from 2003 January 1 to 2015 December 31. Based on these data, we have statistics on the ratio of cloudy-to-clear nights. The information provided distinguishes specific resolution elements as either clear or cloudy. We count the number of cloudy nights and divided by the number of days in that month or year, then get the monthly or annual percentages of cloudy nights. For easier comparison, we convert the percentages of cloudy nights into clear nights, which could result in an overestimation of the clear night percentage if there is a difference in the assignment of cloudy/clear between EOS/TERRA and EOS/AQUA. We assume it is small for the clear night rates of all sites higher than 50% from other satellite data based on the small differences in cloud cover from EOS/TERRA and EOS/TERRA results processed by Cavazzani et al. (2015) and Barnes et al. (2016).

### 2.2.2 MODIS data results

The annual percentage distribution of cloudy nights from MODIS data from 2003 to 2015 is displayed in Figure 2. Similar to the GMS+NOAA data, the percentage of cloud cover in central and southeastern China is high, generally more than 50%. In the vicinity of  $40^\circ$  N, from the middle of Inner Mongolia to the middle of the Xinjiang autonomous region, and the west and middle of the Tibetan Plateau, there are low cloud cover areas. It is clear from the figure that each observatory is in a local low-cloud area, despite the different areas of site selection.

Comparing the cloud data of GMS+NOAA and MODIS, as shown in Figure 2, there is a significant cloud reduction on the west side of  $90^\circ$  E in China, which might

<sup>1</sup> <https://modis-atmos.gsfc.nasa.gov/>

closely relate to the mechanism of cloud formation. A large part of the humid air from the west side of  $90^\circ$  E is brought by the westerlies from the Pamir wet area (Dai 1990; Tian *et al.* 2004; Lioubimtseva *et al.* 2005). The Pamir wet area is located on the southwest side of the Pamirs, with its wet center near Kabul in Afghanistan and Islamabad in Pakistan. The westerlies move eastward, encountering the Iranian Plateau, the Pamirs and the Tibetan Plateau. Due to the blocking effect of the mountains, the westerlies are divided into two branches, which are named the north branch of the westerlies and the south branch of the westerlies. The branch point is located at  $60^\circ$  E.

1. The north branch of the westerlies entering the Tarim Basin converges near the Tibetan Plateau terrain boundary with anticyclonic circulation in the Tarim Basin. This effect resulted in a cloud system on the southwestern edge of the Tarim Basin, which is the cloud system near the Mutztag-ata site (group A).
2. The south branch of the westerlies moves along the Himalayas in the south of the Tibetan Plateau. When the jet is strong, it will rise to the high altitudes of the Himalayas. This effect results in the clouds around Xiangzi, Diya, Ali-F, Ali-D, Ali-A, Huoerba and Payang (group B and C).

The water vapor situation in the Pamir wet area is changing over a long period. According to a study by the Intergovernmental Panel on Climate Change (IPCC), during the 21st century, the inland regions exhibited a gradual trend of increasing drought, especially in subtropical, low latitudes and mid latitudes. More specific observations demonstrate that in Afghanistan and Pakistan, the annual precipitation from 1979 to 2005 manifested a significant decline compared to the average annual precipitation from 1961 to 1990. In our data, the change can be seen when comparing the GMS+NOAA data from 1998 to 2003 in the upper panel of Figure 2 with the MODIS data from 2004 to 2015 plotted on the same scale in the lower panel of Figure 2. Furthermore, based on the SRES A1B scenario, “fifteen-model” indicates the water vapor supplied by the Pamir wet area will significantly reduce, which results in cloud reduction. In all areas impacted by westerlies, the future cloud formation rate will be lower (Bates *et al.* 2008).

From MODIS data, the monthly percentage distribution of cloudy nights accumulated from 2003 to 2015 is displayed in Figure 3. Each subgraph represents the percentage distribution of cloudy nights in each month and all of them are arranged following the seasonal order, starting with March in spring. Most of China is dominated by the East Asian Summer Monsoon. Warm and humid

air from the tropical sea area is abundant in summer, with the high temperature and extensive evaporation giving rise to a period of excessive summer clouds. The monthly average cloud cover in the southeastern and central parts of China is generally higher than 50% during the night. Due to the lower humidity, the nighttime cloud cover from central Inner Mongolia to central Xinjiang and most of Tibet remains at a low level and varies little with the seasons. The cloud cover of the sites in group D is also higher in summer, and lower in winter. Although this phenomenon is the case in most parts of southeastern China, the cloud formation is mainly impacted by the Indian Monsoon in this area.

The significant seasonal changes of clear night percentages in each site are plotted in Figure 4, and the main reason for the changes in western China is the combination of westerlies and monsoons. The wind system in China is mapped in Figure 5, which transports water vapor to condense into clouds under appropriate conditions.

The strength and location of westerlies in China are closely related to the season. In winter, the westerlies are stronger and southerly, with the main direction around the vicinity of  $30^\circ$  N. In summer, the westerlies are weaker and northerly, with the main direction around the vicinity of  $40^\circ$  N (Yi 2011). Therefore, the sites affected by the westerlies have more clouds in winter.

For monsoons in China, the situation is more complex. Three types of monsoon affect the Chinese climate, including the Winter Monsoon from Mongolia, the East Asian Summer Monsoon from the Pacific Ocean and the Indian Monsoon. Warm and humid water vapor in the eastern Indian Ocean passes through the Bay of Bengal and crosses the Yarlung Zangbo to the east of the Tibetan Plateau and is the main element that generates clouds in the western part of China. In the summer, the monsoon winds are stronger, while in the winter, the monsoon winds are weak. Thus, the sites affected by monsoons have more clouds in the summer.

The influence of the westerlies and monsoons can be analyzed in the statistics of the clear sky percentages for each site. Limited by the wind strength and distribution of the westerlies and monsoons, sites in the northwest are susceptible to the westerlies, while sites in the southeast are susceptible to monsoons. Therefore, in group order, A, B, C and D are decreasingly affected by the westerlies and increasingly affected by monsoon. Assuming that the conditions for cloud formation from water vapor in each region remain unchanged, the cloud cover increase in February can be regarded as a sign of influence from the westerlies, and the cloud cover increase in August is a sign of influ-

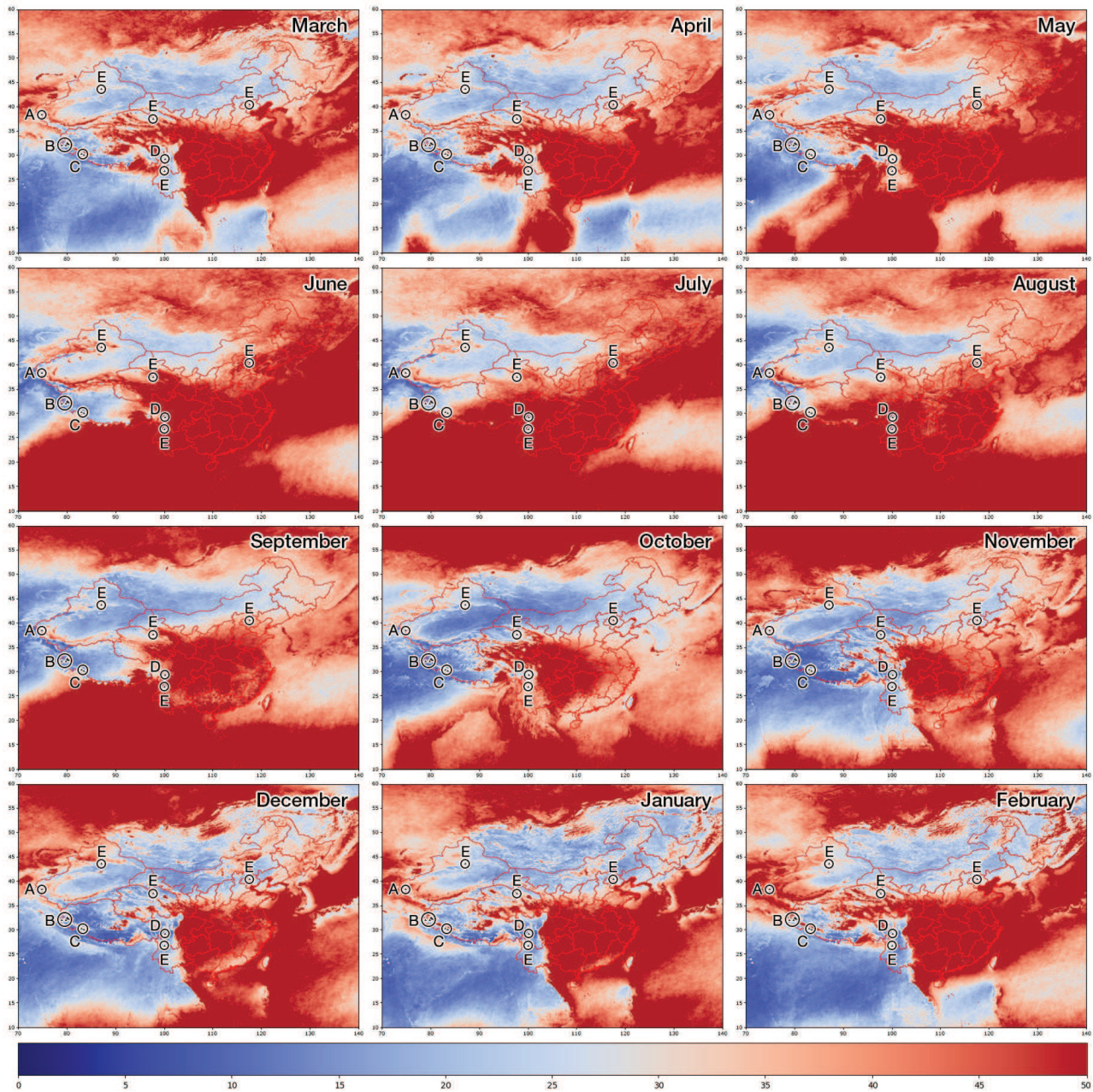


**Fig. 3** The MODIS monthly percentage distribution of cloud cover less than 50%, accumulated from 2003 January 1 to 2015 December 31.

ence from the monsoon. At the same time, the degree of cloud cover can be regarded as a sign of the degree of influence from the westerlies or monsoon. This is illustrated by the spatial distribution of cloud cover in February and August (Figs. 6–7), and the statistics in Figure 4.

As depicted in Figure 8, group B (in the case of Ali-F,  $80.33494^{\circ}\text{E}$ ,  $5125\text{m}$ ) and C (in the case of Payang,  $83.46912^{\circ}\text{E}$ ,  $4600\text{m}$ ) are located north of the Himalayas and south of the Gangdese, with longitudes between  $78^{\circ}\text{E}$  and  $84^{\circ}\text{E}$  and altitudes between  $4621$  and  $5292\text{m}$ . However, groups B and C manifest significantly differen-

t seasonal cloud distributions from the MODIS data. The water vapor situation of group B is more impacted by the westerlies and less by the monsoons; group C sites are almost not affected by the westerlies but mainly by the monsoons. We infer a difference in the cloud formation in the area north of the Himalayas between the east and west side of  $82^{\circ}\text{E}$ .

The most significant landmark near  $82^{\circ}\text{E}$  is Mayum La (marked in Fig. 8), with a longitude of  $82.43429^{\circ}\text{E}$  and a latitude of  $30.63046^{\circ}\text{N}$ , which is signified with a bold black line in Figure 8. It is the watershed between the

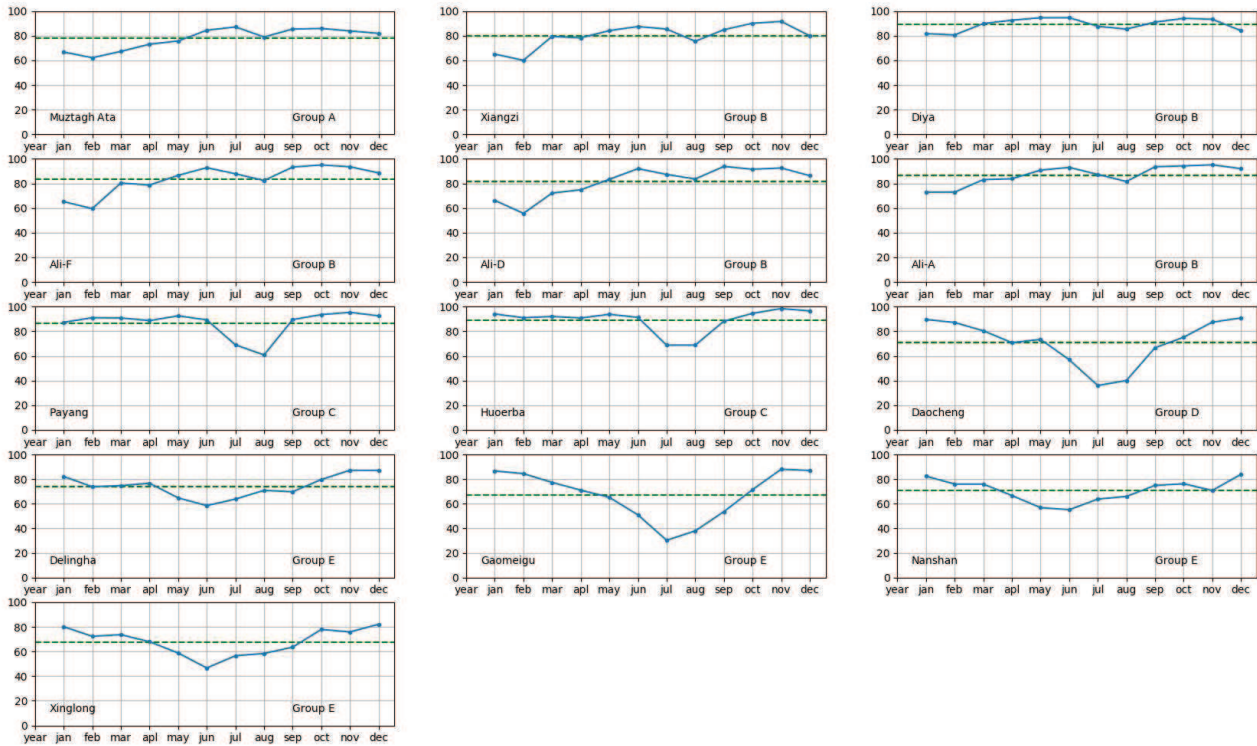


**Fig. 4** Annual trends of MODIS clear night percentage accumulated from 2003 January 1 to 2015 December 31. Each point represents a monthly average percentage of cloud cover.

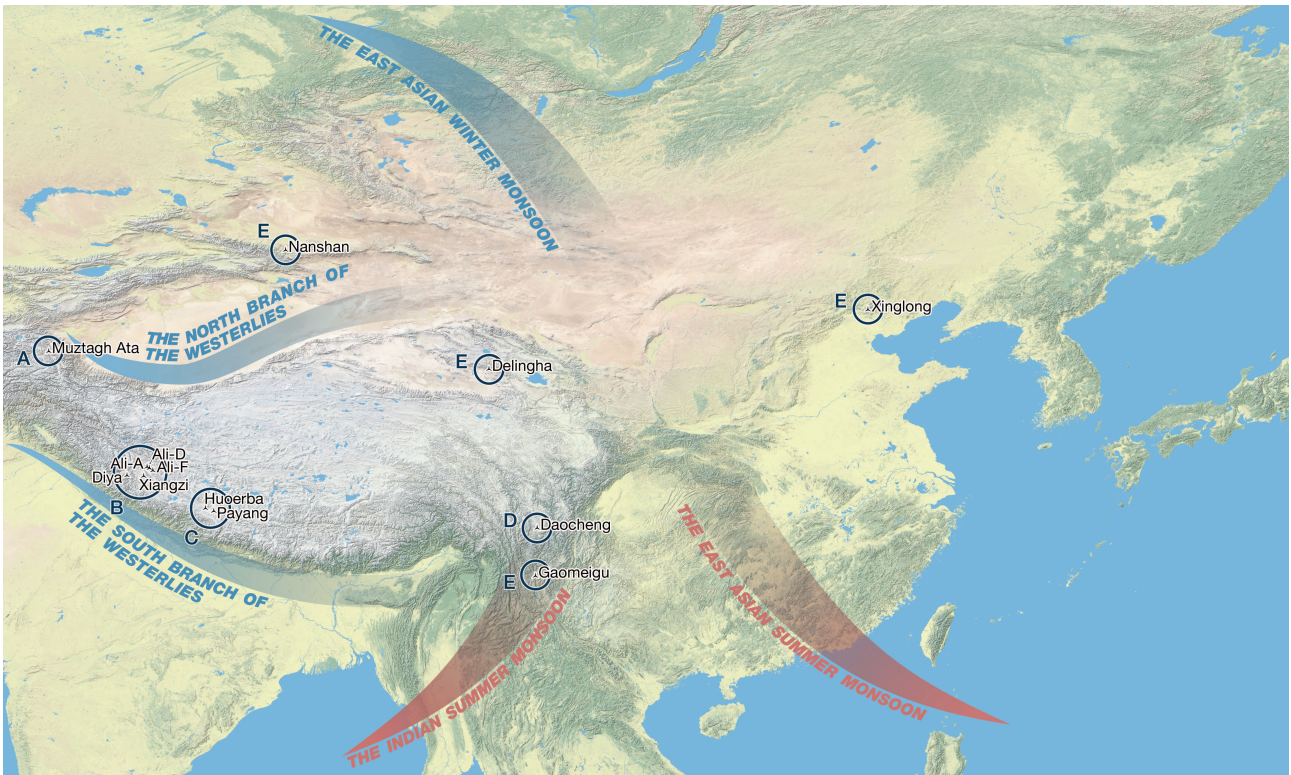


**Fig. 5** The geographical distribution of westerlies and monsoons. The winds highlighted with blue prevail in winter, and the winds signified with red prevail in summer.

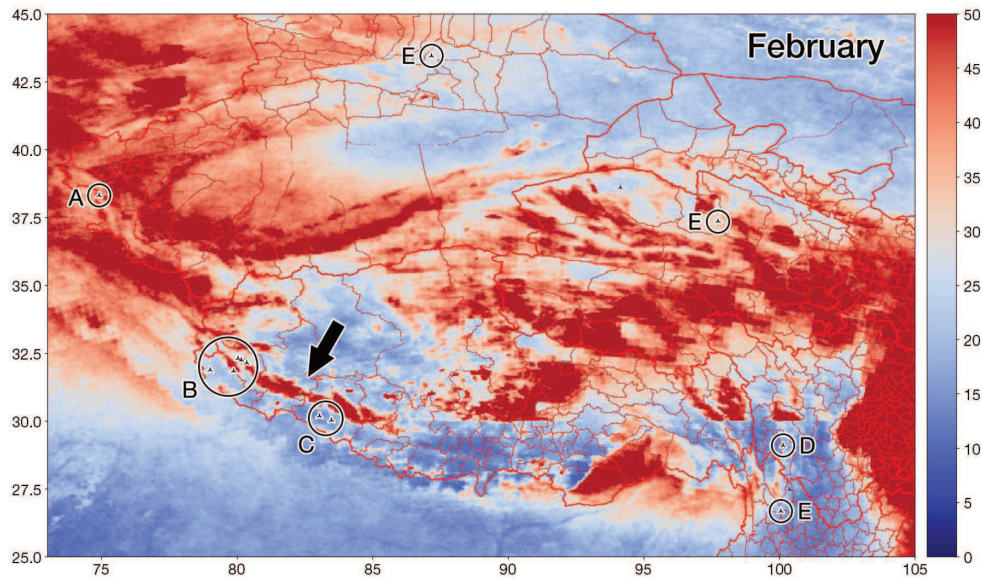


**Fig. 6** The MODIS monthly percentage distribution with less than 50% cloud cover in western China in February. The *black arrow* presents a new cloud strip, not seen in GMS+NOAA.

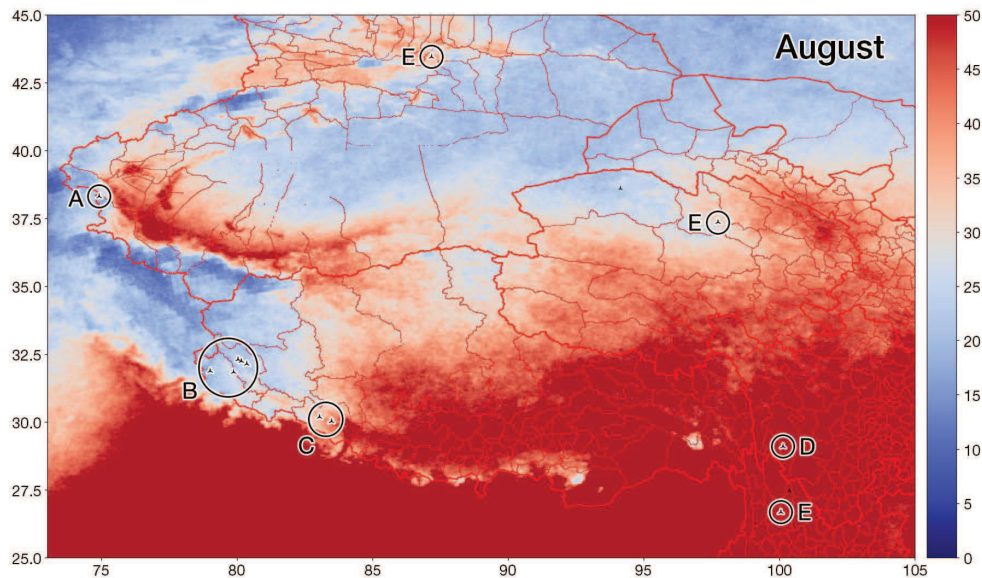


**Fig. 7** The MODIS monthly percentage distribution of cloud cover less than 50% in western China in August.

sources of the Brahmaputra and Indus rivers. The altitude of Mayum La is 5285 m, significantly higher than the average local elevation and appears to significantly weaken the influence of the monsoons from the west. Thus on the west side of Mayum La, the cloud formation is more influenced by the westerlies, whereas on the other hand, on the east side it is dominated by the monsoons.

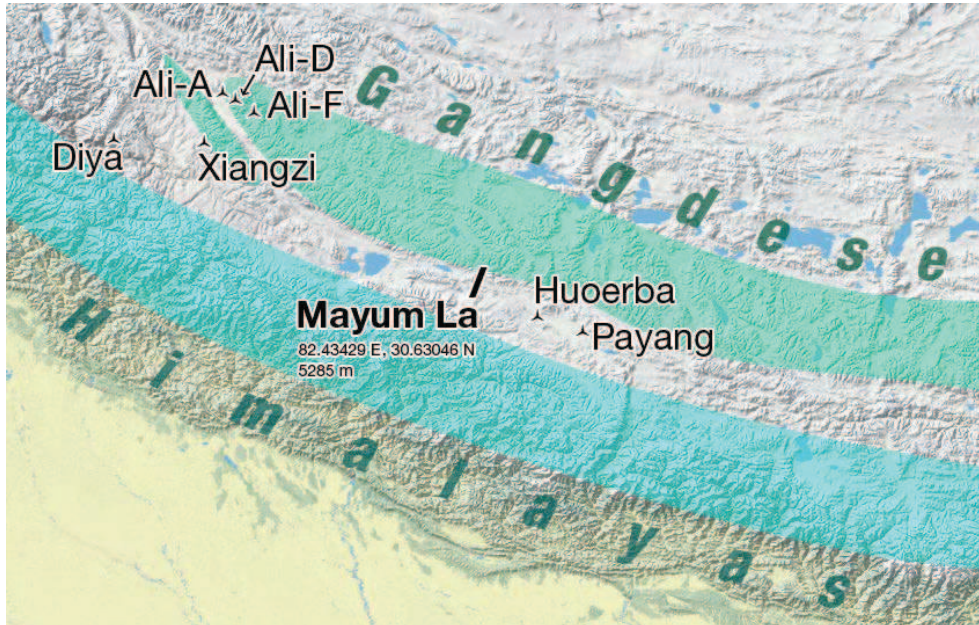
When we compare with the GMS+NOAA data, a new cloud strip (highlighted in Fig. 6 by a black arrow) formed near groups B and C in the MODIS data, which is dis-

tributed in the Gangdese. The cloud strip is evident in winter and disappears in summer, which suggests its formation is affected by the westerlies. Considering the spatial distribution of the GMS+NOAA's annual average cloud cover in Figure 2, the clouds on the west side of the Tibetan Plateau have accumulated in large numbers and have not crossed the Himalayas into China. We can speculate that the westerlies have been significantly enhanced since 2003. This phenomenon is consistent with the IPCC's Fourth Assessment Report, which concluded that

**Table 3** The annual average percentage of clear free nights from NMC MODIS, CAS MODIS, Barnes et al. (2016) MODIS and Cavazzani et al. (2017) MODIS for all sites referred to in this work.

Group	Site	NMC	CAS	Barnes	Cavazzani
		Epoch	2003 – 2015	2003 – 2014	2001 – 2011
A	Muztagh-ata	77.8	78.1	-	-
B	Xiangzi	80.2	-	-	-
B	Diya	89.1	84.2	-	-
B	Ali-F	83.8	-	-	-
B	Ali-D	81.8	-	-	-
B	Ali-A	86.8	82.6	-	-
C	Payang	86.6	82	-	-
C	Huoerba	89.0	-	-	-
D	Daocheng	71.1	71.6	-	-
E	Delingha	74.1	-	-	-
E	Gaomeigu	66.9	-	-	-
E	Nanshan	70.7	-	-	-
E	Xinglong	67.9	68.5	-	-
-	Mauna Kea	-	84.1	88%(TERRA)/84%(AQUA)	-
-	Armazones	-	85.5	-	87.5

The data from Barnes et al. (2016) are from the contour plot in their figs. 2(c) and 2(d) and private communication. The data from Cavazzani et al. (2017) MODIS are written in italic since they are inferred from Table 3 and Fig. 7. It should be noted that diverse definitions of “clear” fraction were used here due to the methods applied, and it should not be confused with the fraction of photometric nights or the time an observatory can be operated at the sites. The relationship with the all-sky camera is discussed by Cao et al. (2020).

**Fig. 8** The location of Mayum La. The cyan and light turquoise colors represent the rough geographical distributions of parts of the Himalayas and Gangdese respectively. Blue signifies lakes.

mid-latitude westerlies have generally increased in both hemispheres (Stocker et al. 2013).

The annual average percentages of clear nights from 2003 to 2015 are shown in Figure 9. The data from groups A, B, C and D are more cloud-free than the currently running observing stations in group E. From Table 4, the annual average cloud cover of the sites in group C is the lowest, while those in group B and A are higher than that in group D. Group A has the most stable annual average cloud cover. On the other hand, the difference between the highest and

lowest in group B is significant, and the standard deviation of group B is 3.31, though it also has the largest number of sites. Aside from a possible slight improvement in clear skies at group C, we note that Figure 10 does not exhibit any particular evidence for any overall trend in site characteristics that might be expected based on Section 2.2. Our analysis suggests that this has a local explanation in that while the overall level of clouds has gone down somewhat, this has been compensated by increased seasonality introduced by local features such as that illustrated in Figure 6.

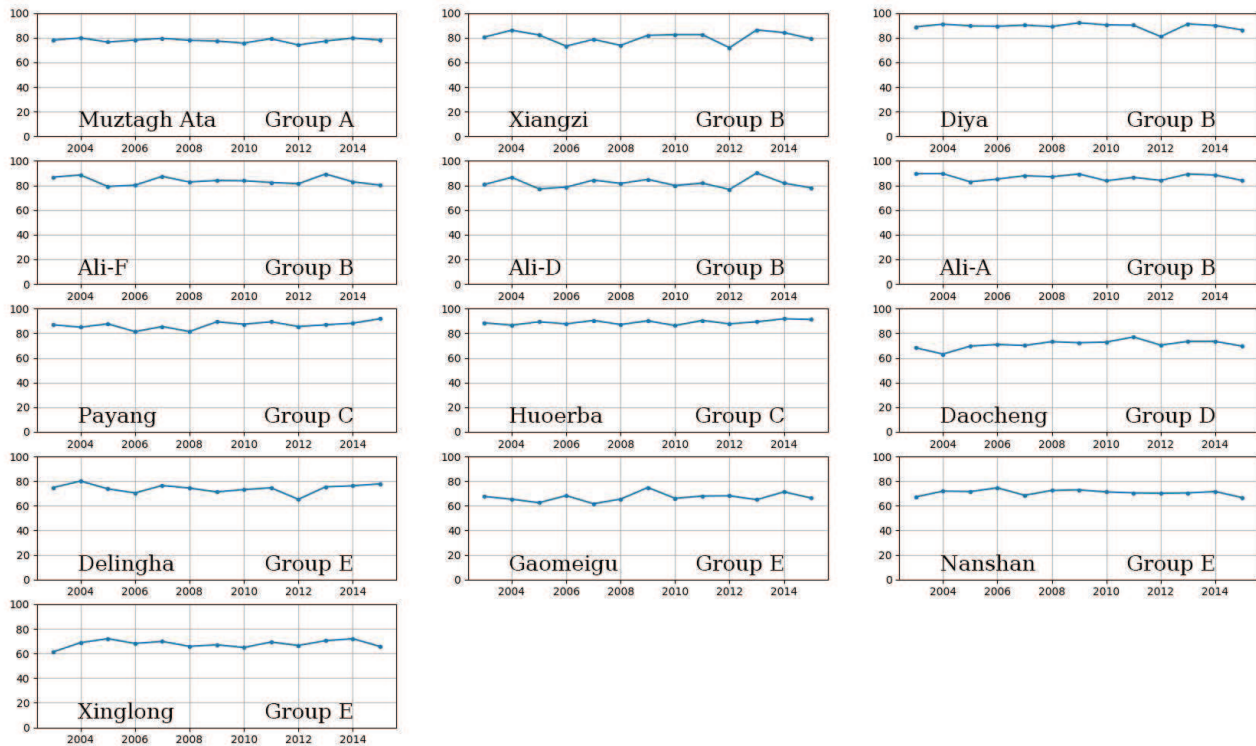


Fig. 9 The MODIS annual average percentages of clear nights from 2003 January 1 to 2015 December 31.

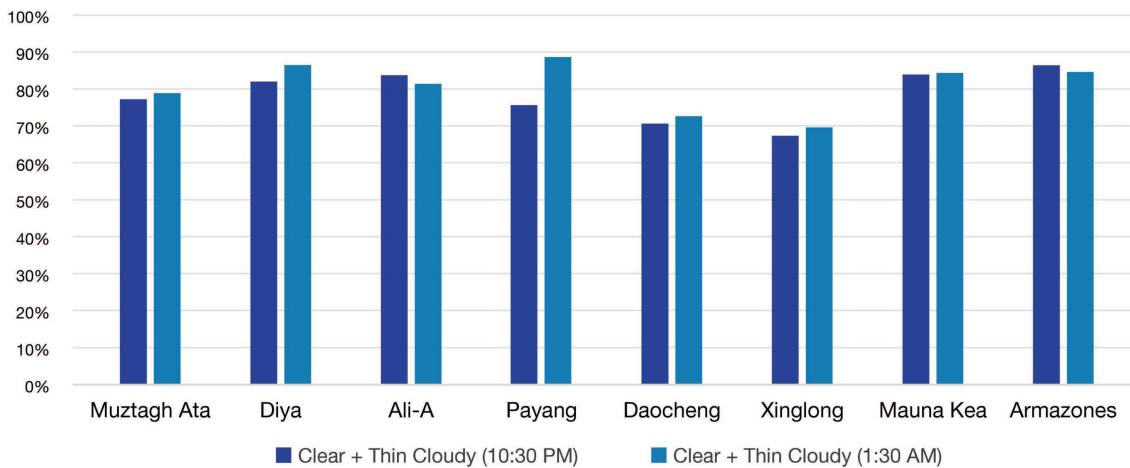


Fig. 10 The probability of clear and thin cloudy cases at 10:30 PM and 1:30 AM (local time) from CAS MODIS. The definitions of the clear and thin cloudy situations are from Liu & Liu (2013).

As expected, the performance of the sites will be related to the local geographical features.

For comparison between the sites in China and TMT/ELT sites, a team from the Institute of Geographic Sciences and Natural Resources Research, Chinese Academy of Sciences processed the MODIS data (CAS MODIS for short) from 2003 to 2014 at eight sites by a different method (Liu & Liu 2013). This method estimates if a pixel corresponds to a cloud or not and then makes further classification about the type of cloud.

Liu & Liu (2013) subdivisions include a “thin cloudy” assignment though it appears that this case is rather sensitive and should be interpreted with caution. In particular, there may be one or more issues related to the ability of the data processing to robustly identify thin clouds: (1) the variable “Angle R37” is overestimated or the parameter of “Reference R37” is underestimated in the workflow of Liu & Liu (2013), (2) the sites are relatively small in comparison with the spatial resolution of the satellite data and to-

**Table 4** Comparison of annual average percentage of cloud-free nights from NMC MODIS and “simplified CAS MODIS” data processing.

Group	NMC	CAS
A	77.2	78.1
B	84.3 ± 3.6	83.4
C	87.8 ± 1.7	82
D	71.1	71.6
E	70.1 ± 3.2	68.5

pographic features of these sites are different from those of their surroundings, and so local details need to be checked.

The CAS MODIS “clear” fractions for Mauna Kea and Cerro Armazones are less than what has been found by a number of long-running experiments. The geographical features of the sites, including being near the ocean (Cavazzani *et al.* 2011), covered by snow and having low altitude mist, will impact results. In certain conditions, such features can introduce a difference in cloud cover of more than 75% (Cavazzani *et al.* 2015). This explanation seems particularly plausible in the case of Mauna Kea given its more varied local geography and climate. If we ignore the CAS MODIS sub-divisions between “clear” and “thin cloudy,” the simplified result is more reasonable. We plot these data in Figure 10, and put “clear” and “thin cloudy” in the same bin with the same color. When we compare the combination of “clear” and “thin cloudy” with the “clear” data from the National Meteorological Center of China (NMC MODIS for short), we conclude that NMC MODIS and so-called “simplified CAS MODIS” are relatively consistent with an average difference of 2% (see Table 3). It can be seen that the simplified CAS MODIS data are very close to cloud-free night percentages found by Barnes *et al.* (2016) and Cavazzani *et al.* (2017) from the MODIS data.

From the simplified CAS MODIS data, the Muztagh-ata from group A, Ali-A and Diya from group B, Payang from group C and Daocheng from group D are all slightly lower than the TMT/ELT sites but higher than Xinglong Observatory. The annual average percentages of cloud-free nights from the MODIS dataset, including NMC MODIS, CAS MODIS, the MODIS values processed by Barnes *et al.* (2016) and the MODIS values processed by Cavazzani *et al.* (2017) are listed in Table 3 and Table 4 and exhibit reasonable consistency with each other. Barnes *et al.* noted that the cloud detection algorithm may over-rely on surface temperature retrievals from MODIS, and there may be a bias in the nighttime cloud cover frequency data toward lower-than-actual cloud cover frequency. In other words, we should regard Table 4 and Figure 11 as representing the maximum percentage of clear nights that might be obtained.

### 3 CONCLUSIONS

In our consideration of suitable astronomical sites in western China, from a meteorological perspective we took into account four low cloud areas around the Tibetan Plateau, including: the northwestern side of the Tibetan Plateau and the southern margin of the Tarim Basin; the eastern side of the Tibetan Plateau, Sichuan, Yunnan and Guizhou; the Great Bend of Yarlung Zangbo; and the west side of the Tibetan Plateau. These result in seasonal changes in the cloud cover in western China and changes influenced by the westerlies and monsoons. We find evidence for the cloud cover reducing in areas affected by the westerlies, which is consistent with the expectations from climate change models.

We identified three groups of sites A, B and C with significant advantages:

Group A is located in the Eastern Pamirs, a series of peaks on the east side of the site, including Kongur Tagh (7719 m), Kongur Tiube (7555 m) and Muztagh-ata (7546 m), though we have only considered the latter of these. The water vapor brought into the Tarim Basin by the westerlies is blocked by these peaks on the east of the site, and leads to a reasonably consistent amount of clear sky throughout the year.

Groups B and C are located at the southwest of the Tibetan Plateau, between the Gangdese and Himalayas, which avoids the unstable air areas caused by high-pressure and low-pressure systems and the winds caused by momentum exchange between high-level and low-level air (Huang & Mao 1994). The area near group C has excellent cloud statistics in this study. However, this area is vulnerable to the negative impact of a potential expansion of the monsoon region due to climate change, which would manifest as a reduced fraction of clear sky in August and surrounding months.

On the whole, the clear nights available in groups A, B and C (~83% on average) are slightly lower than those at the TMT/ELT sites (~85% on average) but higher than what is available at currently operational observatories in China (<70% on average). Further analysis of satellite data and its detailed comparison with ground-based data are required and presented elsewhere in this special edition (e.g., Cao *et al.* 2020).

The cloud cover, as ascertained from satellites, depends on data sources and their processing algorithms: different instruments observing in a specific band reveal various physical characteristics of the clouds; even with identical original data, results interpreted by different algorithms would vary as well. After data analysis and comparison, the results are acceptable in the long-term cloud cover s-

tudy. Moreover, as mentioned before, ground-based observations are essential for identifying candidate sites.

**Acknowledgements** We are very grateful to Jie-Tai Mao for satellite data processing and Mallory Barnes for clarifying details of Barnes et al. The research is partly supported by the Operation, Maintenance and Upgrading Fund for Astronomical Telescopes and Facility Instruments, budgeted from the Ministry of Finance of China (MOF) and administered by the Chinese Academy of Sciences (CAS). The research is also supported by the National Natural Science Foundation of China (Grant Nos. 11573054, 11703065, 11603044 and 11873081). The MODIS data referred to in this research were provided by teams from the National Meteorological Center of China and the Institute of Geographic Sciences and Natural Resources Research, Chinese Academy of Sciences (CAS). HRAJ acknowledges support from a CAS PIFI and UK STFC grant ST/R006598/1.

## References

- Ackerman, S. A., Strabala, K. I., Menzel, W. P., et al. 1998, *Journal of Geophysical Research: Atmospheres*, 103(D24), 32141
- Barnes, M. L., Miura, T., & Giambelluca, T. W. 2016, *Journal of Climate*, 29, 77
- Bates, B., Kundzewicz, Z., Wu, S., & Palutikof J. P. 2008, *Climate Change and Water*, Technical Paper of the Intergovernmental Panel of Climate Change, IPCC Secretariat, Geneva, 210
- Cao, Z. H., Hao, J. X., Feng, L., et al. 2020, *RAA (Research in Astronomy and Astrophysics)*, 80, 82
- Cavazzani, S., Ortolani, S., Zitelli, V., & Maruccia, Y. 2011, *MNRAS*, 411, 1271
- Cavazzani, S., Zitelli, V., & Ortolani, S. 2015, *MNRAS*, 452, 2185
- Cavazzani, S., Ortolani, S., & Zitelli, V. 2017, *MNRAS*, 471, 2616
- Chen, W. 2017, *Satellite Meteorology (3rd ed.)* (China Meteorological Press) in Chinese
- Cui, X., Zhu, Y., Liang, M., et al. 2018, *Proc. of the SPIE*, 10700, 107001P
- Chen, D., Wang, J. C., Xu, J., et al. 2003, *Publications of the Yunnan Observatory*, 95, 1
- Dai, J. 1990, *The climate of Qinghai-Tibet Plateau* (China Meteorological Press) (in Chinese)
- Dim, J. R., Takamura, T., Okada, I., Nakajima, T. Y., & Takenaka, H. 2007, *Journal of Geophysical Research* 112, D13202
- Frey, R. A., Ackerman, S. A., Liu, Y., et al. 2008, *Journal of Atmospheric and Oceanic Technology*, 25(7), 1057
- Huang, Y., & Mao, J. 1994, *Acta Astrophysica Sinica*, 14, 379
- Huang, Y., & Mao, J. 1996, *Astrophysics reports (Pub. Beijing Astronomical Observatory)*, 28, 62
- Kramer, H. J. 2002, *Observation of the Earth and its Environment: Survey of Missions and Sensors* (Springer Science & Business Media)
- Lioubimtseva, E., Cole, R., Adams, J. M., & Kapustin, G. 2005, *Journal of Arid Environments*, 62(2), 285
- Liu, H., Zhu, W., Yi, S., et al. 2003, *Acta Meteorologica Sinica*, 61(4), 465
- Liu, J., Zhang, Y., Feng, G., & Bai, C. 2014, in *Proc. of IAU Symp.*, 298, 427
- Liu, R., & Liu, Y. 2013, *Remote Sensing of Environment*, 133, 21
- Melnick, J., & Monnet, G. 2011, *Revista Mexicana de Astronomía y Astrofísica*, 41, 36
- Menzel, W. P., Frey, R. A., Zhang, H., et al. 2008, *Journal of Applied Meteorology and Climatology*, 47(4), 1175
- Platnick, S., King, M. D., Ackerman, S. A., et al. 2003, *IEEE Transactions on Geoscience and Remote Sensing*, 41(2), 459
- Qian, X., Yao, Y. Q., & Zhang, Y. J. 2012, *Acta Astronomica Sinica*, 53, 426
- Rodgers, C. D. 1976, *Reviews of Geophysics*, 14(4), 609
- Schöck, M., et al. 2009, *PASP*, 121, 384
- Schöck, M., Nelson, J., Els, S., et al. 2011, *Revista Mexicana de Astronomía y Astrofísica*, 41, 32
- Stocker, T. F., Qin, D., Plattner, G. K., et al. 2013, in *Climate Change 2013: The Physical Science Basis* (Cambridge University Press), 867
- Stubenrauch, C. J., Rossow, W. B., Kinne, S., et al. 2013, *Bulletin of the American Meteorological Society*, 94(7), 1031
- Tian, H., Guo, P., & Lu, W. 2004, *Journal of Tropical Meteorology*, 20(4), 401 (in Chinese)
- Tian, J. F., Deng, L. C., Zhang, X. B., et al. 2016, *Publications of the Astronomical Society of the Pacific*, 128(968), 105003
- Weng, D., & Han, A. 1998, *Journal of Applied Meteorological Science*, 9(1), 32 (in Chinese)
- Yi, S. 2011, *Climate Change – Geophysical Foundations and Ecological Effects*, eds, J. Blanco, & H. Kheradmand, 157
- Zhang, J. C., Ge, L., Lu, X. M., et al. 2015, *Publications of the Astronomical Society of the Pacific*, 127(958), 1292
- Zhang, Y., Wang, P., & Yao, Y., et al. 2010, *Scientia Sinica (Physica, Mechanica & Astronomica)*, 40, 1302